# Climate model response from the Geoengineering Model Intercomparison Project (GeoMIP)

Ben Kravitz,[1] Ken Caldeira,[2] Olivier Boucher,[3] Alan Robock,[4] Philip J. Rasch,[1] Kari Alterskjær,[5] Diana Bou Karam,[6] Jason N. S. Cole,[7] Charles L. Curry,[8] James M. Haywood,[9,10] Peter J. Irvine,[11] Duoying Ji,[12] Andy Jones,[9] Jón Egill Kristjánsson,[5] Daniel J. Lunt,[13] John C. Moore,[12] Ulrike Niemeier,[14] Hauke Schmidt,[14] Michael Schulz,[15] Balwinder Singh,[1] Simone Tilmes,[16] Shingo Watanabe,[17] Shuting Yang,[18] and Jin-Ho Yoon[1]

Received 7 January 2013; revised 3 July 2013; accepted 10 July 2013.

[1] Solar geoengineering—deliberate reduction in the amount of solar radiation retained by the Earth—has been proposed as a means of counteracting some of the climatic effects of anthropogenic greenhouse gas emissions. We present results from Experiment *G1* of the Geoengineering Model Intercomparison Project, in which 12 climate models have simulated the climate response to an abrupt quadrupling of $CO_2$ from preindustrial concentrations brought into radiative balance via a globally uniform reduction in insolation. Models show this reduction largely offsets global mean surface temperature increases due to quadrupled $CO_2$ concentrations and prevents 97% of the Arctic sea ice loss that would otherwise occur under high $CO_2$ levels but, compared to the preindustrial climate, leaves the tropics cooler ($-0.3$ K) and the poles warmer (+0.8 K). Annual mean precipitation minus evaporation anomalies for *G1* are less than 0.2 mm day$^{-1}$ in magnitude over 92% of the globe, but some tropical regions receive less precipitation, in part due to increased moist static stability and suppression of convection. Global average net primary productivity increases by 120% in *G1* over simulated preindustrial levels, primarily from $CO_2$ fertilization, but also in part due to reduced plant heat stress compared to a high $CO_2$ world with no geoengineering. All models show that uniform solar geoengineering in *G1* cannot simultaneously return regional and global temperature and hydrologic cycle intensity to preindustrial levels.

**Citation:** Kravitz, B., et al. (2013), Climate model response from the Geoengineering Model Intercomparison Project (GeoMIP), *J. Geophys. Res. Atmos.*, *118*, doi:10.1002/jgrd.50646.

## 1. Introduction

[2] Much of the climate change experienced since the mid-twentieth century is very likely due to anthropogenic emissions of greenhouse gasses [*IPCC*, 2007]. While virtually eliminating net greenhouse gas emissions is the only permanent method of addressing climate change, there are several proposed ideas for lessening the effects of global warming by reducing the amount of sunlight incident at the surface, which we call solar geoengineering [e.g., *Budyko*, 1974; *Crutzen*, 2006; *Wigley*, 2006]. For example, surface cooling

Additional supporting information may be found in the online version of this article.

[1]Pacific Northwest National Laboratory, Richland, Washington, USA.
[2]Department of Global Ecology, Carnegie Institution for Science, Stanford, California, USA.
[3]Laboratoire de Météorologie Dynamique, IPSL, CNRS/UPMC, Paris, France.
[4]Department of Environmental Sciences, Rutgers University, New Brunswick, New Jersey, USA.
[5]Department of Geosciences, University of Oslo, Oslo, Norway.
[6]Laboratoire des Sciences du Climat et de l'Environnement, CEA/CNRS/UVSQ, Saclay, France.

Corresponding author: B. Kravitz, Pacific Northwest National Laboratory, PO Box 999, MSIN K9-24, Richland, WA 99352, USA. (ben.kravitz@pnnl.gov)


2169-897X/13/10.1002/jgrd.50646

[7]Canadian Centre for Climate Modeling and Analysis, Environment Canada, Toronto, Ontario, Canada.
[8]School of Earth and Ocean Sciences, University of Victoria, Victoria, British Columbia, Canada.
[9]Met Office Hadley Centre, Exeter, UK.
[10]College of Engineering, Mathematics and Physical Sciences, University of Exeter, Exeter, UK.
[11]Institute for Advanced Sustainability Studies, Potsdam, Germany.
[12]State Key Laboratory of Earth Surface Processes and Resource Ecology, College of Global Change and Earth System Science, Beijing Normal University, Beijing, China.
[13]School of Geographical Sciences, University of Bristol, Bristol, UK.
[14]Max Planck Institute for Meteorology, Hamburg, Germany.
[15]Norwegian Meteorological Institute, Oslo, Norway.
[16]National Center for Atmospheric Research, Boulder, Colorado, USA.
[17]Japan Agency for Marine-Earth Science and Technology, Yokohama, Japan.
[18]Danish Meteorological Institute, Copenhagen, Denmark.

**Table 1.** Models Participating in GeoMIP That Have Thus Far Completed Experiment *G1*[a]

| Model | Atmosphere Model | Ocean Model | Land Model |
|---|---|---|---|
| BNU-ESM | CAM3.5 (T42/L26; 42 km) | MOM4p1 (200 boxes × 360 boxes) | CoLM (T42/L10) *Dai et al.* [2003, 2004] |
| CanESM2 | (T63/L35; 1 hPa/69 km[b]) *Arora et al.* [2011] | (0.94° × 1.4°/L40) | CLASS 2.7 and CTEM 1.0 (T63/L3) *Arora and Boer* [2010]; *Verseghy et al.* [1993] |
| CESM-CAM5.1-FV | CAM5 (1.875° × 2.5°/L30; 40 km) | POP2 (1° × 1°/L60) *Smith et al.* [2010] | CLM4 (0.9° × 1.25°) *Oleson et al.* [2010] |
| CCSM4 *Gent et al.* [2011] | CAM4 (0.9° × 1.25°/L28; 42 km) | POP2 (1° × 1°/L60) *Smith et al.* [2010] | CLM4 (0.9° × 1.25°) *Oleson et al.* [2010] |
| EC-Earth *Hazeleger et al.* [2011] | IFS (T159/L62; 5 hPa/53 km[b]) | NEMO (1° × 1°/L42) *Madec*, 2008 | |
| GISS-E2-R *Schmidt et al.* [2006] | ModelE2 (2° × 2.5°/L40; 80 km) | Russell (1° × 1.25°/L32) *Russell et al.* [1995] | GISS-LSM (2° × 2.5°/L6) *Aleinov and Schmidt* [2006] |
| HadCM3 *Gordon et al.* [2000] | (2.5° × 3.75°/L19; 30 km) | (1.25° × 1.25°/L20) | MOSES 1 (2.5° × 3.75°/L4) |
| HadGEM2-ES *Collins et al.* [2011] | HadGEM2-A (1.25° × 1.875°/L38; 40 km) *HadGEM2 Dev. Team* [2011] | HadGEM2-O (1/3-1°/L40) *HadGEM2 Dev. Team* [2011] | MOSES-II *Essery et al.* [2003] |
| IPSL-CM5A-LR *Dufresne et al.* [2013] | LMDz (2.5° × 3.75°/L39; 65 km) *Hourdin et al.*, 2012 | NEMO (96 boxes × 95 boxes/L39) *Madec*, [2008] | ORCHIDEE *Krinner et al.* [2005] |
| MIROC-ESM *Watanabe et al.* [2011] | MIROC-AGCM (T42/L80; 0.003 hPa/127 km[b]) *Watanabe et al.* [2008] | COCO3.4 (0.5−1.4° × 1.4°/L44) *K-1 model developers*, 2004 | MATSIRO (T42/L6) *Takata et al.* [2003] |
| MPI-ESM-LR *Giorgetta et al.* [2013] | ECHAM6 (T63/L47; 0.01 hPa/115 km[b]) *Stevens et al.* [2013] | MPIOM (1.5° × 1.5°/L40) *Marsland et al.* [2003] | JSBACH *Raddatz et al.* [2007] |
| NorESM1-M *Alterskjær -et al.* [2012] | CAM-Oslo (1.9° × 2.5°/L26; 2 hPa/62 km[b]) *Kirkevåg et al.* [2013] | (based on) MICOM (~1° × 1°/L70) *Assmann et al.* [2010] | CLM4 *Oleson et al.* [2010] |

[a]For each column, the name of the specific model is given, along with a reference (where available). Numbers in parentheses describe the horizontal resolution of in degrees or number of grid boxes (lat × lon) or number of spectral elements (*T*)/number of vertical layers (*L*); and height of the model top (km or hPa, atmosphere only).

[b]denotes model top heights that were converted from pressure using a scale height of 10 km.

could theoretically be achieved by creating a large sunshade in space, mimicking volcanic eruptions by injecting large amounts of sulfate aerosols into the stratosphere, or by brightening marine stratocumulus clouds [*Shepherd et al.*, 2009].

[3] Several multimodel comparisons of solar geoengineering have been performed, but intercomparability was limited, either due to models performing different experiments [*Rasch et al.*, 2008] or only a small number of models being included, each showing different results [*Jones et al.*, 2010]. The Geoengineering Model Intercomparison Project (GeoMIP) proposed four computer modeling experiments involving reductions in solar irradiance or increased stratospheric loading of aerosols to determine robust features of climate model responses to solar geoengineering [*Kravitz et al.*, 2011a, 2011b]. These four proposed computer modeling experiments all build on the Coupled Model Intercomparison Project Phase 5 (CMIP5) framework [*Taylor et al.*, 2012].

[4] Preliminary studies using GeoMIP simulations were performed by *Schmidt et al.* [2012b], who studied the results of Experiment *G1* (described below) in four models, three of which are participants in the Implications and Risks of Engineering Solar Radiation to Limit Climate Change project [*Schmidt et al.*, 2012a]. Our study is the first to analyze Experiment *G1* for the full set of GeoMIP models. Participation is currently 12 fully coupled atmosphere-ocean general circulation models (Table 1), 11 of which have dynamic vegetation; we discuss this in more detail in section 3.3. This broad participation allows us to address robust features of the impact of solar geoengineering as simulated by climate models, focusing on temperature, radiation, sea ice extent, the hydrologic cycle, and terrestrial net primary productivity. In particular, this multimodel ensemble encompasses a wide breadth of parameterizations and included processes, adding strength to our conclusions about the robust responses found in climate model simulations of solar geoengineering.

## 2. Study Design and Analysis Methods

[5] All simulations in each model are initiated from a preindustrial control run that has reached steady state; we denote this simulation *piControl*, which is the standard CMIP5 name for this experiment [*Taylor et al.*, 2012]. Our reference simulation, denoted *abrupt4xCO2*, is one in which the $CO_2$ concentration is instantaneously quadrupled from the control run. Experiment *G1* involves an instantaneous reduction of insolation on top of this $CO_2$ increase such that 10 year mean globally averaged top of atmosphere (TOA) radiation differences between *G1* and *piControl* are no more than 0.1 W m$^{-2}$ for the first 10 years of the 50 year experiment [*Kravitz et al.*, 2011a, 2011b]. The amount of solar radiation reduction is model-dependent (Table 2) but does not vary during the course of the simulation. This step-function change in solar intensity is intended to approximately offset the radiative forcing resulting from the step-function change in atmospheric $CO_2$ concentration.

[6] Experiment *G1* is idealized, which has allowed broad participation and facilitates intercomparison. All 12 modeling groups that have participated in GeoMIP thus far have performed this experiment. Based on the CMIP5 *abrupt4xCO2* experiment, *G1* starts from a stable preindustrial climate and imposes two large counteracting step-function forcings,

**Table 2.** Changes in Insolation and Planetary Albedo for Each Model[a]

| Experiment<br>Year | $S_0$ Reduction (%)<br>*G1* | Planetary Albedo (%)<br>*piControl* | *abrupt4xCO2*<br>1 | *abrupt4xCO2*<br>50 | *G1*<br>1 | *G1*<br>50 |
|---|---|---|---|---|---|---|
| BNU-ESM | 3.8 | 29.8 | 29.2 | 28.4 | 29.3 | 29.2 |
| CanESM2 | 4.0 | 29.5 | 28.8 | 28.5 | 28.9 | 29.0 |
| CCSM4 | 4.1 | 28.7 | 28.1 | 27.9 | 28.1 | 28.0 |
| CESM-CAM5.1-FV | 4.7 | 29.6 | 29.3 | 28.3 | 29.3 | 29.2 |
| EC-Earth | 4.3 | 29.1 | 28.6 | 28.2 | 28.8 | 28.8 |
| GISS-E2-R | 4.5 | 29.5 | 29.4 | 29.7 | 29.4 | 29.2 |
| HadCM3 | 4.1 | 29.8 | 28.9 | 28.8 | 29.0 | 28.9 |
| HadGEM2-ES | 3.9 | 28.7 | 28.2 | 27.5 | 28.0 | 27.9 |
| IPSL-CM5A-LR | 3.5 | 30.7 | 29.6 | 28.3 | 30.0 | 29.9 |
| MIROC-ESM | 5.0 | 31.3 | 30.2 | 29.4 | 30.1 | 30.4 |
| MPI-ESM-LR | 4.7 | 30.2 | 29.4 | 28.9 | 29.4 | 29.4 |
| NorESM1-M | 4.0 | 30.8 | 30.3 | 30.1 | 30.3 | 30.1 |

[a]Column 2 shows the solar reduction required in *G1* to balance the TOA radiative effect from *abrupt4xCO2* for each model. Column 3 shows the initial planetary albedo before $CO_2$ or solar forcings are added. Columns 4–7 show planetary albedo in years 1 and 50 (annual average), as a first-order indication of changes in cloud cover due to the experiments *abrupt4xCO2* and *G1*. All values are given in % and are rounded to 1 decimal place.

preventing many problems with weak signal-to-noise ratios. Moreover, changes in solar forcing are uniformly parameterized in models as a change in TOA downwelling radiation, whereas differing treatment of sulfate aerosols in each model will be a dominating complication of the intercomparison for some of the GeoMIP experiments.

[7] This experiment is the most idealized GeoMIP simulation, facilitating unambiguous analysis of the dominant radiative effects and climate responses. *Ammann et al.* [2010] showed that uniform solar constant reduction yields a similar pattern of radiative forcing and temperature response to a suitably thick layer of stratospheric sulfate aerosols, although solar reduction and stratospheric aerosols have different effects in terms of stratospheric heating, dynamic circulation patterns, and stratospheric chemistry. As such, while insights into the likely response to uniform solar geoengineering can be obtained, modeling a reduction in solar irradiance cannot serve as a substitute for simulating the response to increased stratospheric aerosols or other possible approaches for reducing incoming solar radiation.

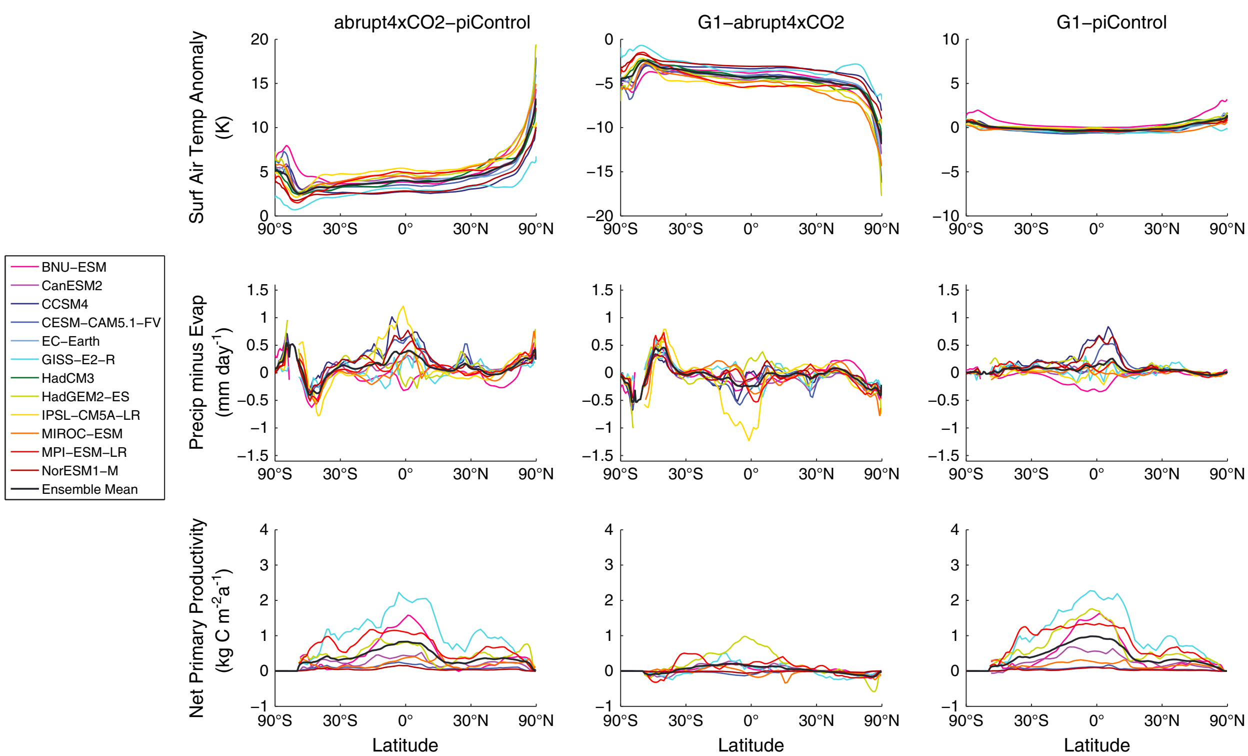


**Figure 1.** Zonal average anomalies in surface air temperature (K; land + ocean average; 12 models), precipitation minus evaporation (mm day$^{-1}$; land average; 12 models), and terrestrial net primary productivity (kg C m$^{-2}$ year$^{-1}$; land average; 8 models) for all available models. All values shown are averages over years 11–50 of the simulations. The *x* axis is weighted by cosine of latitude.

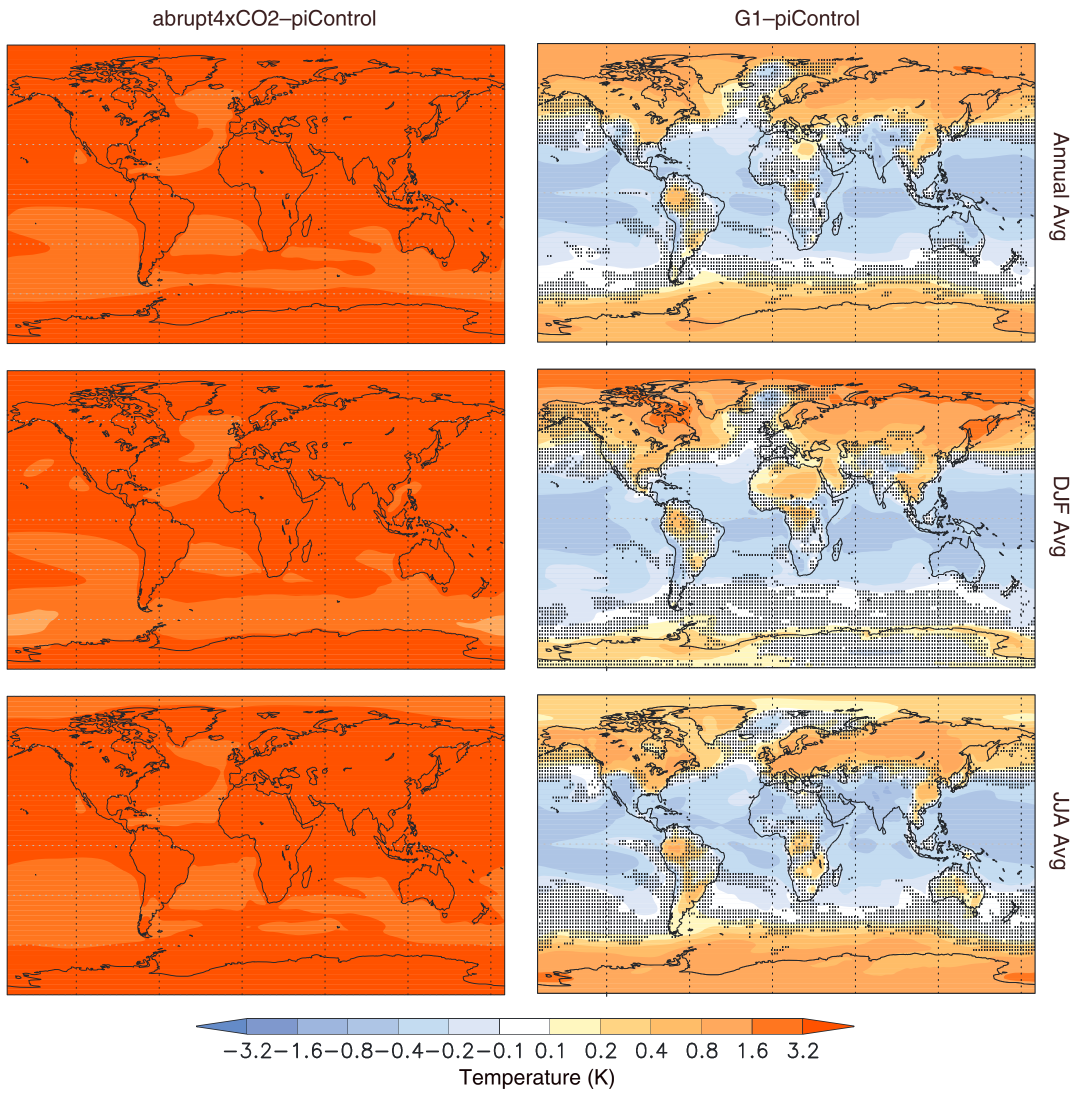


**Figure 2.** All-model ensemble annual average surface air temperature differences (K) for *abrupt4xCO2–piControl* (left column) and *G1–piControl* (right column), averaged over years 11–50 of the simulation. Top row shows annual average, middle row shows December-January-February (DJF) average, and bottom row shows June-July-August (JJA) average. Stippling indicates where fewer than 75% of the models (for this variable, 9 out of 12) agree on the sign of the difference.

[8] All values are reported as mean (min to max) where mean represents the all-model ensemble average, and min and max are results from the ensemble member that exhibits the minimum and maximum value, respectively, for the quantity of interest. Unless otherwise noted, all values presented are averages over years 11–50 of the simulation. Available variables from the models that were used to create ensemble averages are presented in Table S1. All maps and zonal averages in both the article and supplemental online material show values for the all-model ensemble average, averaged over years 11–50 of the simulation. Land-only averages do not include areas containing sea ice.

[9] The experimental design results in small temperature changes (*G1–piControl*), which have the effect of suppressing temperature-related feedbacks in the climate system, reducing model spread. To avoid conflating reasons for model agreement in our study with reasons for model agreement in projections of future climate change, we chose to apply a stippling criterion in which stippling denotes areas where fewer than 75% of models agree on the sign of the model response. In our figures, we assign no color to values that are small, but some of these areas may not be stippled, indicating widespread model agreement. This could be either due to many models showing small changes that by chance happen to have the same sign or lack of stippling could be the result of a small number of disagreeing models that have differences that are large in magnitude.

[10] Throughout the paper and in Tables S2–S4, we refer to particular geographical regions. The tropics are defined as the regions bounded by the Tropics of Capricorn and Cancer, i.e., the area between 23.44°S and 23.44°N. The Arctic is defined as all area north of the Arctic Circle, i.e., the area between 66.55°N and 90°N. The Antarctic is defined similarly, i.e., the area between 90°S and 66.55°S. Collectively, the Arctic and Antarctic are referred to as the polar regions. Midlatitudes are defined as the areas between the tropics and the polar regions.

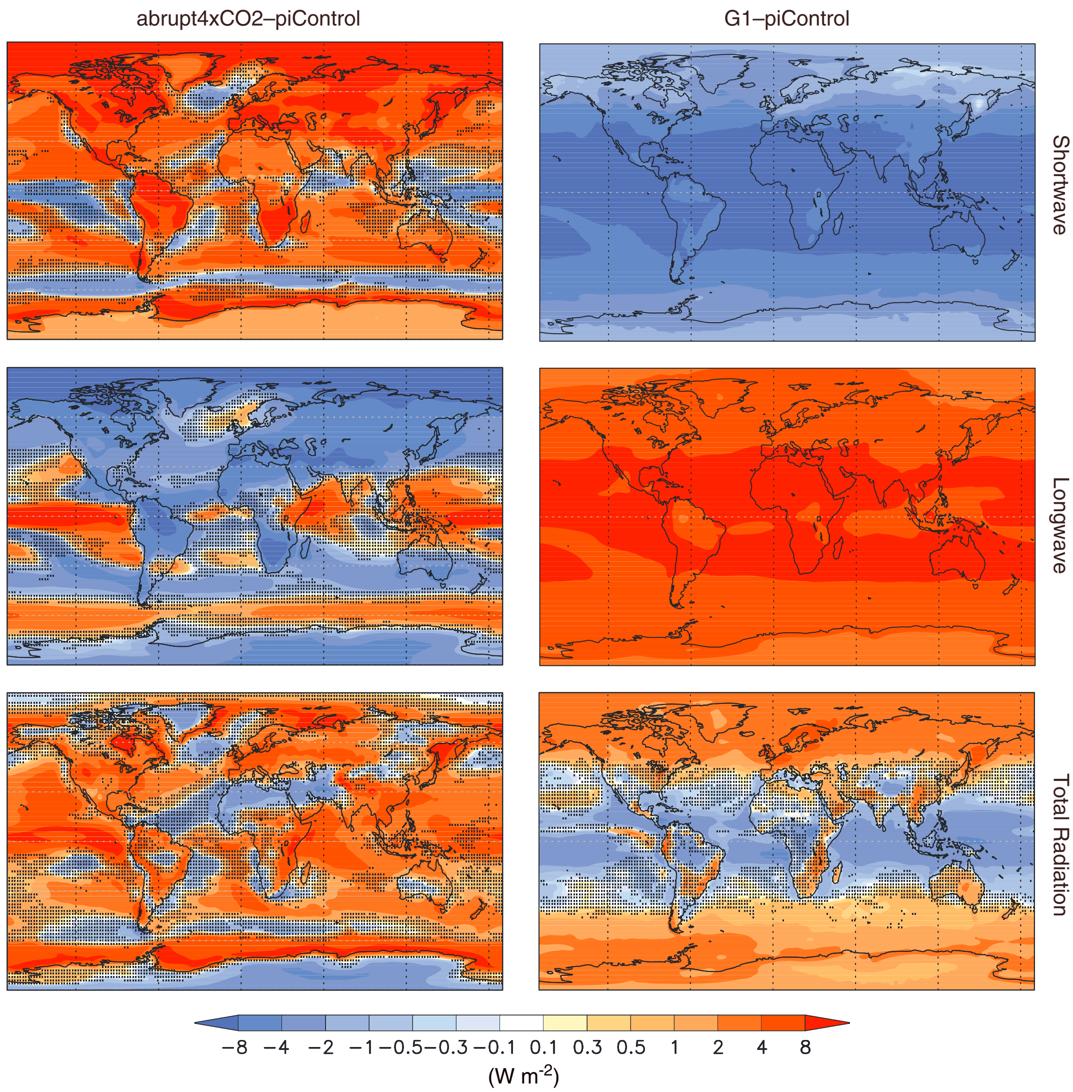


**Figure 3.** All-model ensemble annual average top of atmosphere (TOA) radiation differences (W m$^{-2}$) for *abrupt4xCO2–piControl* (left column) and *G1–piControl* (right column), averaged over years 11–50 of the simulation. Top row shows net shortwave radiation, middle row shows net longwave radiation, and bottom row shows total (shortwave + longwave) radiation. The downward direction is defined to be positive. Stippling indicates where fewer than 75% of the models (for this variable, 9 out of 12) agree on the sign of the difference.

## 3. Robust Responses

### 3.1. Temperature and Radiation

[11] In Experiment *G1*, which is the focus of the analysis in this paper, globally averaged net downward TOA radiation differences from *piControl* are 0.05 (−0.22 to 0.40) W m$^{-2}$ over years 11–50 of simulation [*Kravitz et al.*, 2011a, 2011b]. Because these simulations were initialized from the *piControl* simulation, and the top of atmosphere energy imbalance has been near zero throughout the simulation, it might be expected that globally averaged surface air temperature would show few differences from *piControl* (Figures S1–S3). However, spatial temperature differences (*G1–piControl*) range from −0.3 (−0.6 to 0.1) K in the tropics to 0.8 (0.0 to 2.3) K in the polar regions (Figures 1 and 2 and S4–S6)—results are similar to those found in earlier studies [*Govindasamy and Caldeira*, 2000; *Lunt et al.*, 2008; *Ammann et al.*, 2010]. In particular, the Arctic shows residual warming of 1.0 (−0.3 to 2.9) K, although this residual is small compared to the *abrupt4xCO2–piControl* temperature increases of 10.5 (5.8 to 13.8) K. Polar temperature differences in *G1* are greater during winter than during summer (Figure 2).

[12] The temperature patterns described above are primarily due to unequal distributions of shortwave and longwave radiation from solar reduction and increased $CO_2$ concentration, respectively. The all-model ensemble mean shows net TOA radiation differences (*G1–piControl*) of −1.5 (−2.3 to −0.6) W m$^{-2}$ in the tropics and 2.4 (1.9 to 3.1) W m$^{-2}$ at the poles (Figure 3). Insolation has a latitudinally and seasonally dependent pattern, so any reductions in solar radiation will show similar dependencies. In particular, solar reduction by a fixed fraction will reduce downward shortwave flux by a greater amount in the tropics than at

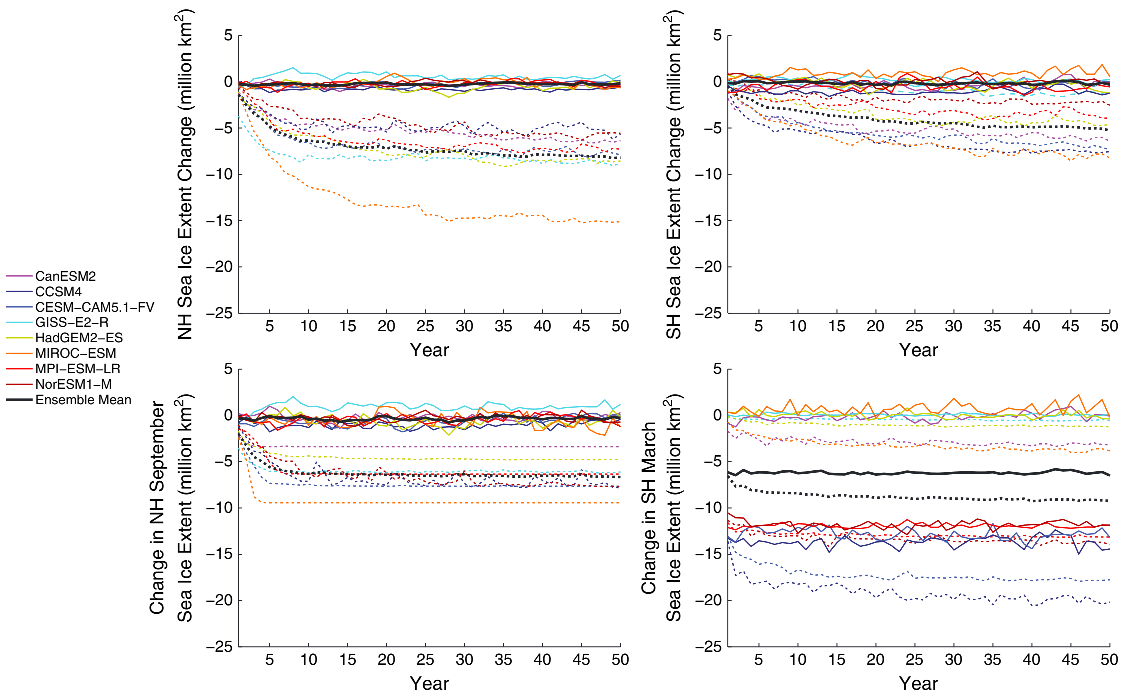


**Figure 4.** Hemisphere-averaged sea ice extent (million km$^2$) for available models (Table S1). Dashed lines indicate *abrupt4xCO2–piControl*, and solid lines indicate *G1–piControl*. Top left shows annually averaged Northern Hemisphere (NH) sea ice extent, top right shows annually averaged Southern Hemisphere (SH) sea ice extent, bottom left shows September NH sea ice extent, and bottom right shows March SH sea ice extent.

the poles and will not reduce downward shortwave flux at all at the dark winter pole. However, carbon dioxide is a well-mixed gas and thus has a more uniform radiative forcing with latitude [*Govindasamy and Caldeira*, 2000].

[13] Table 2 shows a decrease in planetary albedo in experiments *abrupt4xCO2* and *G1*. In the first year of *abrupt4xCO2*, after a step-function change in $CO_2$ concentration, planetary albedo decreases by 0.006, in large part due to a decrease in cloud cover. As the planet warms in this simulation, the albedo change further decreases on average to 0.012 by year 50. In *G1*, solar geoengineering does little to abate the fast response of the climate system to added $CO_2$, so the albedo also decreases in this simulation by an average of 0.006 in year 1. However, because temperature changes are greatly diminished, the year 50 albedo decrease remains approximately 0.006. These decreases in planetary albedo are, in part, indicative of reduced cloud cover. *Ramanathan et al*. [1989] found that cloud radiative forcing is weak in the tropics but has a strong cooling influence in the Northern midlatitudes and a warming influence near both poles. *Zelinka et al*. [2012] found that cloud feedbacks are positive in the midlatitudes and negative poleward of 50°S and 70°N. The cooling in the tropics/midlatitudes and warming at the poles (Figure 2) may in part be associated with reduced cloud cover, consistent with these findings of *Ramanathan et al.* [1989] and *Zelinka et al*. [2012].

[14] Models show some disagreement in *G1–piControl* in the region of approximately 30°–45° in latitude, where the sign of the mean model response changes from positive to negative. Different models will undergo this sign change in different grid boxes, so model agreement would not be expected in these regions. However, models agree on the sign of the temperature response over 74% of the globe and in radiation over 66% of the globe.

[15] A test of the effectiveness of geoengineering in this experiment is the ability of *G1* to restore the climate to that of *piControl* on a local as well as global basis. One measure of this ability to restore climate can be calculated using root-mean-square error. More specifically, we can define the quantity (and other similar quantities)

$$\mathrm{RMS}^{T}_{G1\text{–}piControl} = \sqrt{\frac{\sum\sum (G1\text{-}piControl)^2 \mathrm{d}A}{\sum\sum \mathrm{d}A}}$$

where $T$ denotes temperature (or some other field of interest, averaged over years 11–50 of simulation), *G1* refers to temperature in a particular grid box of the ensemble mean of Experiment *G1*, *piControl* refers to temperature in a particular grid box of the ensemble mean of Experiment *piControl*, summation is over latitude and longitude, and d$A$ denotes the area of a particular grid box (Tables S5–S7). We then calculate the quantity

$$r(T) = \frac{\mathrm{RMS}^{T}_{G1\text{–}piControl}}{\mathrm{RMS}^{T}_{abrupt4xCO2\text{–}piControl}}$$

to determine the effectiveness of *G1* in offsetting the temperature increases under *abrupt4xCO2* on a grid cell basis. This metric has been used in prior geoengineering studies [e.g., *Ban-Weiss and Caldeira*, 2010; *Rasch et al*., 2009]. In this example, $r(T) = 0.089$, indicating a residual of 8.9% of the temperature changes from *abrupt4xCO2* remain under *G1*.

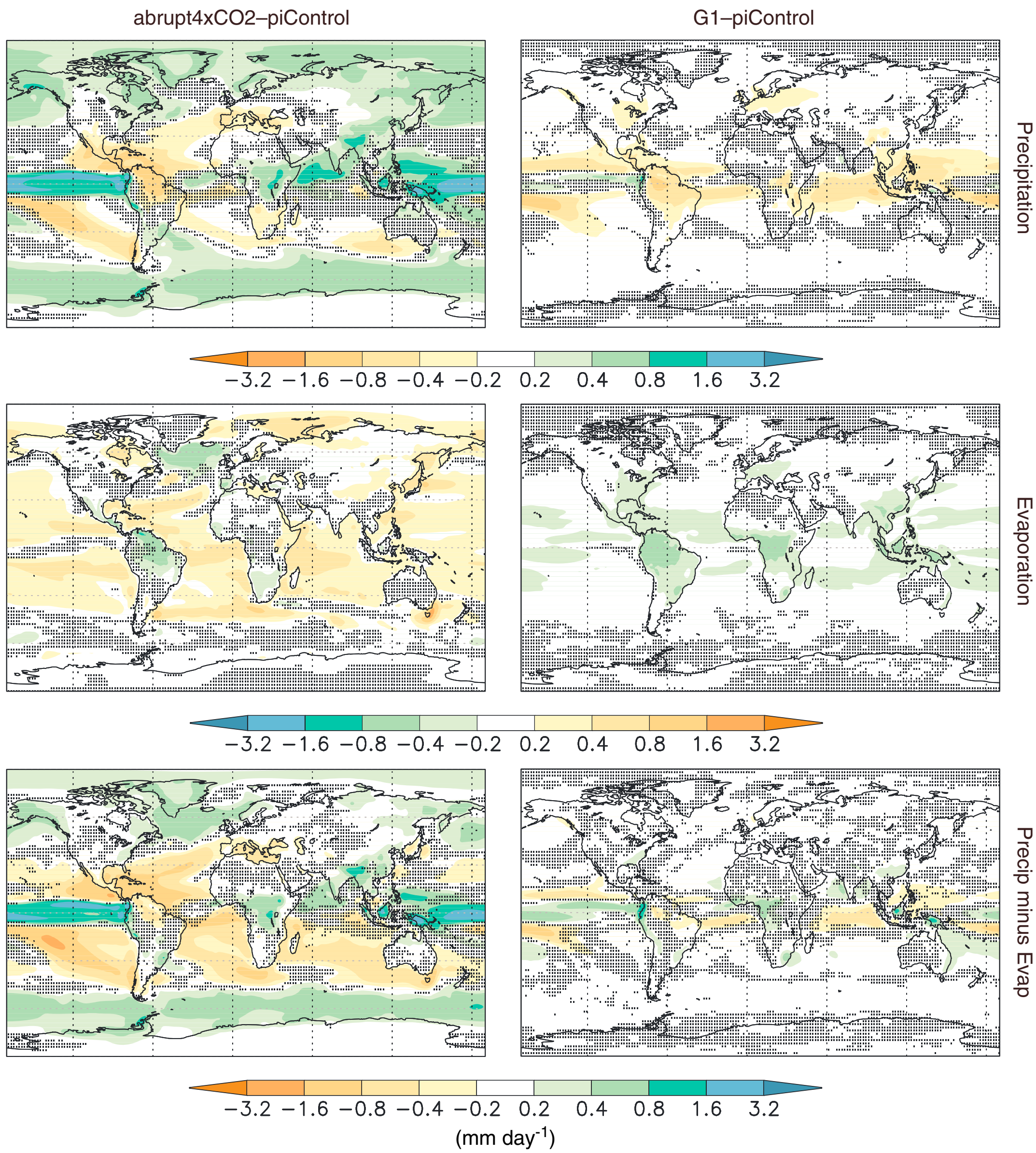


**Figure 5.** All-model ensemble annual average hydrology differences (mm day$^{-1}$) for *abrupt4xCO2–piControl* (left column) and *G1–piControl* (right column), averaged over years 11–50 of the simulation. Top row shows precipitation, middle row shows evaporation, and bottom row shows precipitation minus evaporation. Stippling indicates where fewer than 75% of the models (for this variable, 9 out of 12) agree on the sign of the difference.

*Schmidt et al.* [2012b] show a similar result, i.e., root-mean-square changes in temperature for *G1–piControl* are an order of magnitude smaller than changes for *abrupt4xCO2–piControl*.

### 3.2. Sea Ice

[16] Figure 4 shows model results for Northern and Southern Hemisphere sea ice extent. Because different models simulate sea ice processes in different ways, there is large diversity in the simulated sea ice extent changes in *abrupt4xCO2–piControl* [*Stroeve et al.*, 2012]. Annually averaged Arctic sea ice changes in *abrupt4xCO2* by −7.6 (−14.1 to −5.0) million km$^2$ but stays relatively constant in *G1* with differences from *piControl* of −0.3 (−0.8 to 0.5) million km$^2$. Thus, prevented Arctic sea ice loss in *G1* is 97% (83 to 106). The Antarctic shows similar behavior; annually averaged Southern Hemisphere sea ice extent changes by −4.5 (−7.1 to −1.0) million km$^2$ in *abrupt4xCO2* and −0.2 (−1.1 to 0.9) million km$^2$ in *G1*. Thus, prevented Antarctic sea ice loss by *G1* is 96% (84 to 113). Model agreement and *r* metrics (defined in the previous section) are not reported, as such quantities would depend upon the boundary of sea ice extent, which varies among models.

[17] September Arctic sea ice extent shows similar behavior to the annual average. All models show a large decrease in *abrupt4xCO2*, with some models becoming ice-free in the Arctic. In *G1*, changes in September sea ice are of a similar magnitude to changes in the annual mean.

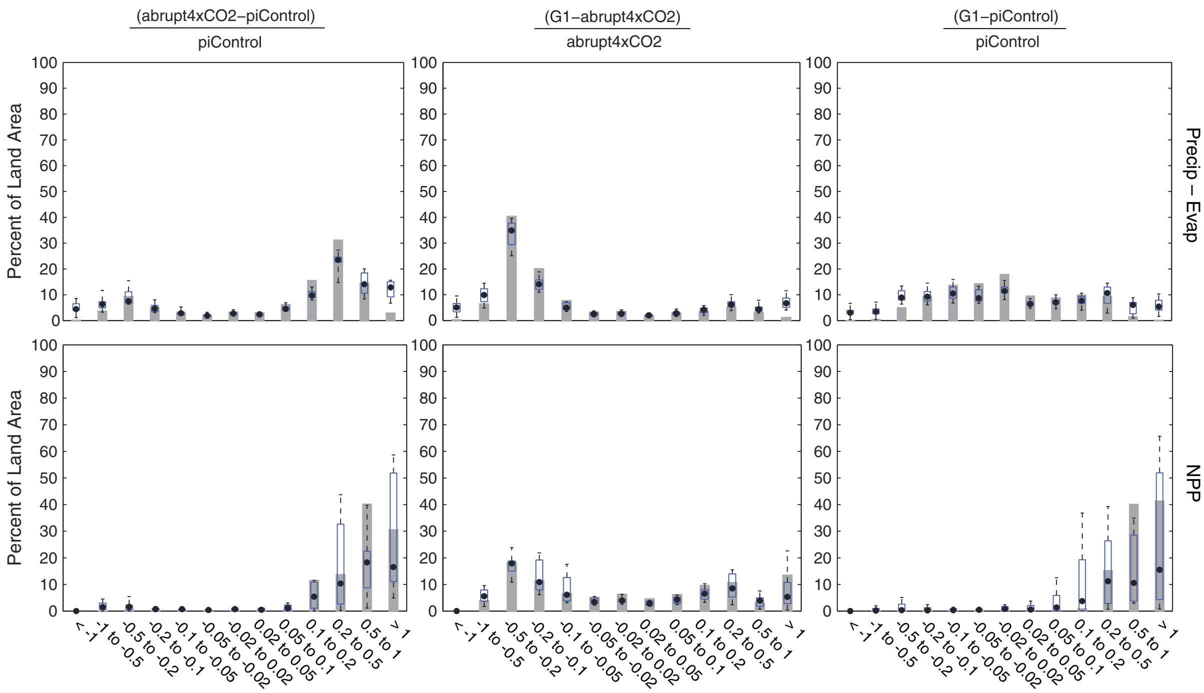


**Figure 6.** Box plot showing the percentage of land area (*y* axis) that undergoes different amounts of relative change (*x* axis) in precipitation minus evaporation (top row) and terrestrial net primary productivity (bottom row). Relative change is given by the formulas at the top of each column. In each bin, black dots indicate the median response of the models, bottom and top of boxes indicate the first and third quartiles of the models, respectively, and whiskers indicate the minimum and maximum model response. Grey bars indicate the response of the all-model ensemble median, which is calculated at each grid point and then sorted into bins. All values shown are for averages over years 11–50 of the simulations.

March Antarctic sea ice extent shows very little model agreement, with some models showing large decreases for both *abrupt4xCO2* and *G1*, and some showing small changes for both simulations.

### 3.3. Hydrology

[18] Global differences (*G1–piControl*) are $-0.1$ ($-0.2$ to $-0.1$) mm day$^{-1}$ for precipitation (4.5% reduction in the all-model ensemble mean), $-0.1$ ($-0.2$ to 0.0) mm day$^{-1}$ for evaporation (4.5% reduction in the all-model ensemble mean), and 0.0 mm day$^{-1}$ for precipitation minus evaporation (*P–E*). Greater than 75% of models agree on the sign of changes (*G1–piControl*) in precipitation throughout 69% of the globe and 61% of the land surface. For evaporation, this agreement is higher; models agree over 81% of the globe and 75% of the land surface. For *P–E*, agreement is over 58% of the globe and 44% of the land surface. Precipitation and evaporation patterns for *G1* and *abrupt4xCO2* are similar and opposite in sign (Figures 1 and 5, and S1–S6), resulting in small differences (*G1–piControl*; $<0.2$ mm day$^{-1}$) in *P–E* over 92% of the globe and 91% of the land surface (Figure 6). The exception is that tropical precipitation is reduced by $-0.2$ ($-0.4$ to $-0.1$) mm day$^{-1}$. These results were also found by *Schmidt et al*. [2012b], in that precipitation responds strongly to both a $CO_2$ increase and a solar reduction, resulting in small differences in the global average for *G1–piControl*.

[19] Figure 7 compares the results in Figure 5 to their natural variability, that is, differences (*G1–piControl*) are divided by the grand standard deviation ($\sigma$) of *piControl* calculated for all models, where each year of each ensemble member of each model is an independent degree of freedom. In regions where annually averaged precipitation in *piControl* is greater than 0.2 mm day$^{-1}$, that is, regions that are not large deserts, changes (*G1–piControl*) in precipitation are within 1.96 $\sigma$ (statistically significant at the 95% confidence level, assuming a normal distribution of differences) of the *piControl* all-model ensemble mean over 96% of the globe and 96% of the land surface. Similarly, changes in *P–E* are within 1.96 $\sigma$ over 91% of the globe and 91% of the land surface. Evaporation shows a statistically significant decrease ($>1.96$ $\sigma$) over 97% of the globe and 90% of the land surface. Evaporation over land is reduced in part due to stomatal closure resulting from increased water use efficiency by plants under increased $CO_2$ concentration [e.g., *Field et al*., 1995; *Sellers et al*., 1996; *Cao et al*., 2010]. Although most of the models do include this process, we did not perform a control experiment that could be used to isolate the stomatal effect. *Fyfe et al*. [2013] presented compelling evidence that these processes are as important as radiative effects on the hydrologic cycle.

[20] The largest differences (*G1–piControl*) in hydrological variables occur in the tropics (Tables S2–S4). Tropical precipitation differences are $-0.2$ ($-0.4$ to $-0.1$) mm day$^{-1}$, tropical evaporation differences are $-0.2$ ($-0.4$ to $-0.1$) mm day$^{-1}$, and tropical *P–E* differences are 0.1 ($-0.2$ to 0.3) mm day$^{-1}$. *Bala et al*. [2008] proposed a mechanism whereby solar reduction results in reduced tropical precipitation; insolation reduction results in greater surface than midtropospheric cooling, which increases atmospheric

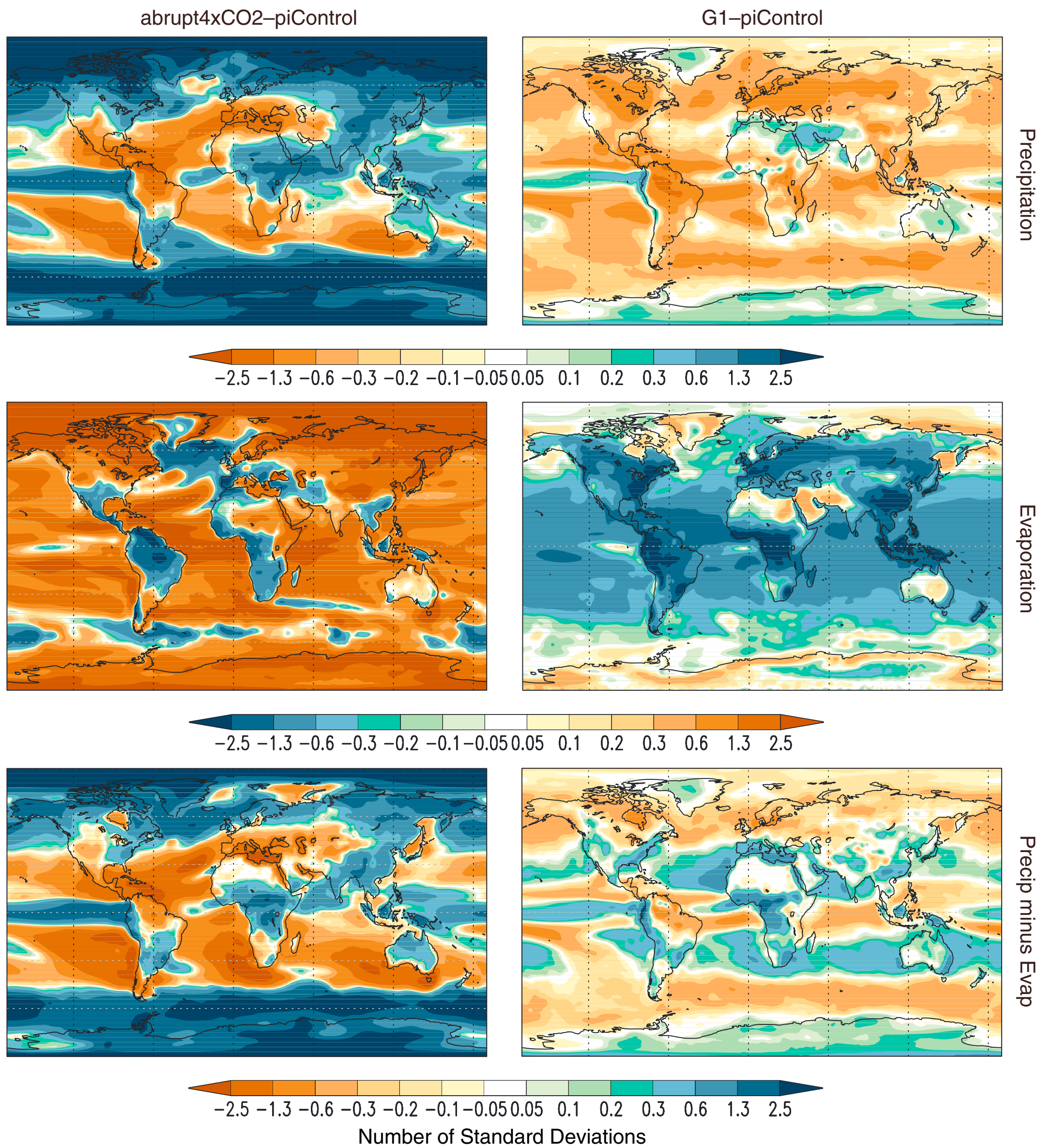


**Figure 7.** Anomalies in annual averages (averaged over years 11–50 of the simulation) divided by the grand standard deviation of *piControl* calculated for all models, where each year of each model is an independent degree of freedom. Left column is *abrupt4xCO2–piControl*, and right column is *G1–piControl*. Top row is precipitation, middle row is evaporation, and bottom row is *P–E*. All values are in numbers of standard deviations. Values shown are anomalies in relation to the natural variability of those fields.

stability, hence suppressing convection. Figure 8 shows calculations of moist static stability for the all-model ensemble mean. More specifically, equivalent potential temperature ($\theta_e$) is given by

$$\theta_e \approx \left(T + \frac{L_v}{c_p} q\right) \left(\frac{p_0}{p}\right)^{R_d/c_p}$$

where $T$ is temperature (K), $L_v$ is an average value of latent heat of vaporization of water ($2.5 \times 10^6\,\mathrm{J\,kg^{-1}}$), $c_p$ is the specific heat of water ($1004\,\mathrm{J\,kg^{-1}\,K^{-1}}$), $q$ is specific humidity ($\mathrm{kg\,kg^{-1}}$), $p_0$ is surface pressure ($\sim 10^5$ Pa), $p$ is pressure (Pa), and $R_d$ is the ideal gas constant for dry air ($287.0\,\mathrm{J\,kg^{-1}\,K^{-1}}$). The all-model ensemble mean of $\frac{\partial \theta_e}{\partial z}$ for most of the troposphere (pressure range of 1000–200 mb) is plotted in Figure 8. If moist static stability increases, this quantity will be positive.

[21] Moist static stability changes for *abrupt4xCO2–piControl* show a reduction in moist static stability throughout the troposphere, particularly in the tropics (Figure 8). This would have the effect of increasing tropical convection, which can lead to increased precipitation, as is seen in the model results for *abrupt4xCO2–piControl* (Figures 5 and S4–S6). These results regarding decreased static stability are consistent with observations [*Huntington*, 2006] and model results [*Held and Soden*, 2006] that show an intensification of the hydrologic cycle accompanying increased atmospheric $CO_2$ concentration. Conversely, differences in

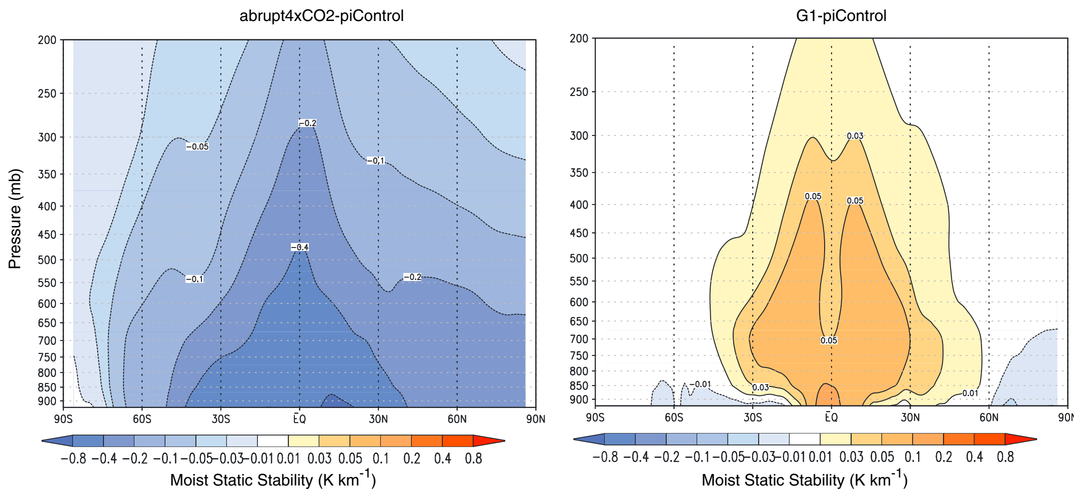


**Figure 8.** All-model ensemble annual average differences in moist static stability (K km$^{-1}$) as defined by $\frac{\partial\theta_e}{\partial z}$, averaged over years 11–50 of the simulations. Left panel shows *abrupt4xCO2–piControl*, and right panel shows *G1–piControl*. Positive values indicate increased stability. Values shown are vertically interpolated.

*G1–piControl* show an increase in moist static stability in the tropical troposphere, a result that is consistent with the mechanism proposed by *Bala et al.* [2008]. *Bony et al.* [2013] find that precipitation changes in *abrupt4xCO2* are consistent with these mechanisms. Thus, *abrupt4xCO2* causes an increase in precipitation in areas that already receive large amounts of precipitation, but *G1* shows the opposite pattern; analysis of monsoon regions shows similar results [*S. Tilmes*, personal communication].

[22] As done for surface air temperature in section 3.1, we can calculate the ability of Experiment *G1* to offset changes in hydrology due to *abrupt4xCO2*. Again denoting $P$ as precipitation and $E$ as evaporation, $r(P) = 0.451$, $r(E) = 0.607$, and $r(P–E) = 0.340$. Thus, a residual of 34% of the $P–E$ changes due to quadrupling of the $CO_2$ concentration remains under *G1*. This result is qualitatively similar to the results of *Ricke et al.* [2010] and *Moreno-Cruz et al.* [2012], namely that uniform solar geoengineering cannot offset both temperature and hydrology changes from an increase in the carbon dioxide concentration.

[23] The reported changes in the hydrologic cycle were calculated using monthly mean model output that has been averaged over years 11–50 of the simulations. However, extreme events manifest on shorter time scales and can have substantial impacts that may not be represented in monthly means.

### 3.4. Terrestrial Net Primary Productivity

[24] The terrestrial biosphere is a significant component of the global carbon cycle and is a large sink for atmospheric $CO_2$ [*Schimel*, 1995]. Net primary productivity (NPP) is defined as the conversion of $CO_2$ into dry matter by the terrestrial biosphere, often calculated as gross primary productivity minus autotrophic respiration [*Cramer et al.*, 1999]. NPP is an indicator of the health of the terrestrial biosphere and its ability to take up $CO_2$. This particular metric is useful for our study, as it integrates changes in radiation, temperature, and moisture into a single aggregate metric that allows us to diagnose the effects of Experiment *G1* on terrestrial carbon balance. NPP can also provide a first-order estimate of the impacts of solar geoengineering on agriculture [*Pongratz et al.*, 2012].

[25] Differences in the three experiments (*piControl*, *abrupt4xCO2*, and *G1*) isolate different mechanisms that determine changes in terrestrial NPP. Changes in NPP for *abrupt4xCO2–piControl* are primarily due to the $CO_2$ fertilization effect on plants, i.e., plants tend to increase productivity in a higher concentration of $CO_2$ [e.g., *Field et al.*, 1995; *Sellers et al.*, 1996; *Cao et al.*, 2010]. Changes for *G1–piControl* are due to a combination of the $CO_2$ fertilization effect and changes in the spatial distributions of temperature and precipitation. Changes for *G1–abrupt4xCO2* are due to changes in spatial distributions of temperature and precipitation alone, of which a prominent component is a reduction in plant heat stress [*Govindasamy et al.*, 2002; *Naik et al.*, 2003; *Pongratz et al.*, 2012]. In particular, this experiment does not change the distribution of direct versus diffuse solar radiation, as occurs in stratospheric sulfate aerosol geoengineering [*Robock*, 2000]. In experiments involving stratospheric sulfate aerosol layers, an increase in the diffuse radiation component may increase NPP [e.g., *Mercado et al.*, 2009].

[26] Changes in NPP for *G1–piControl* are 0.34 (0.0 to 0.8) kg C m$^{-2}$ a$^{-1}$ or 51.0 (4.1 to 121.3) Pg C a$^{-1}$ (Figures 1 and 9, and S1–S6) and are compared to *piControl* values of 43.4 (22.4 to 69.1) Pg C a$^{-1}$, which is of a similar magnitude to reported values in the established literature [*Cramer et al.*, 1999; *Potter et al.*, 2012], constituting a 120% increase in terrestrial NPP. Changes for *abrupt4xCO2–piControl* are 0.3 (0.0 to 0.8) kg C m$^{-2}$ a$^{-1}$, or 49.2 (6.5 to 125) Pg C a$^{-1}$, and patterns of increase in NPP are similar between *G1–piControl* and *abrupt4xCO2–piControl* (Figure 9), implying most of the increase in NPP seen in *G1–piControl* is due to the $CO_2$ fertilization effect. However, *G1–abrupt4xCO2* shows changes in NPP of 0.0 (0.0 to 0.1) kg C m$^{-2}$ a$^{-1}$, or 1.8 (−5.8 to 18.3) Pg C a$^{-1}$, suggesting *G1* has an advantage in increasing terrestrial NPP over *abrupt4xCO2* by providing an environment with enriched $CO_2$ while avoiding the large changes in

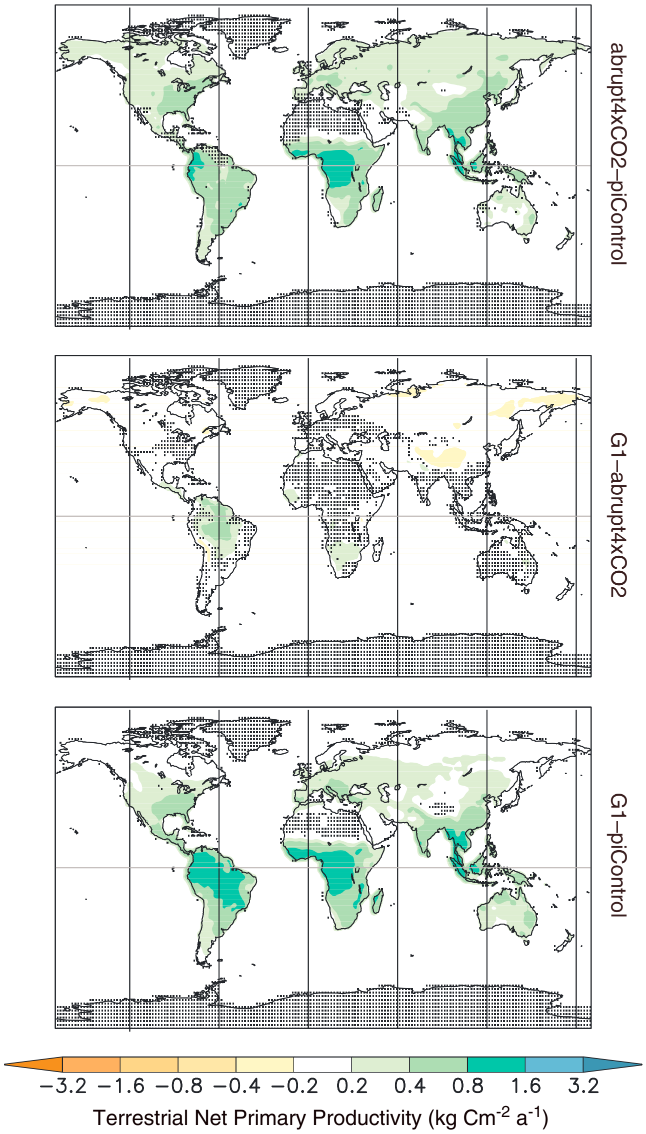


**Figure 9.** All-model ensemble annual average differences in terrestrial net primary productivity (kg C m$^{-2}$ a$^{-1}$), averaged over years 11–50 of the simulation. Top panel shows *abrupt4xCO2–piControl*, middle panel shows *G1–abrupt4xCO2*, and bottom panel shows *G1–piControl*. Stippling indicates where fewer than 75% of the models (for this variable, 6 out of 8) agree on the sign of the difference.

temperature or available moisture (*P–E*) that occur in *abrupt4xCO2*. At least 75% of the models agree on the sign of the response (*G1–piControl*) of NPP over 82% of the land surface. The all-model ensemble mean shows increases in NPP occur over 99% of land regions for *G1–piControl*, 99% of land regions for *abrupt4xCO2–piControl*, and 55% of land regions for *G1–abrupt4xCO2* (Figure 6).

## 4. Conclusions

[27] We have identified several robust results for model predictions of GeoMIP Experiment *G1*, which involves a 4x$CO_2$ atmosphere with a uniform reduction in insolation to produce a near-zero globally averaged TOA net radiation flux. Models agree that although globally averaged surface air temperature may be nearly kept at preindustrial levels, the tropics will be cooler than in *piControl* (0.3 K) and the poles will be warmer than in *piControl* (0.8 K). *G1* is effective at preventing the Arctic sea ice loss that occurs in *abrupt4xCO2*. Changes (*G1–piControl*) in precipitation and *P–E* are within natural variability for 96% and 91% of the globe, respectively, but evaporation shows a statistically significant reduction over 97% of the globe. Tropical precipitation is reduced due to an increase in tropospheric moist static stability. Net primary productivity increases in *G1* by 51.0 Pg C a$^{-1}$, a 120% increase over preindustrial levels; most of the increase is due to $CO_2$ fertilization, but an increase by 1.8 Pg C a$^{-1}$ in *G1–abrupt4xCO2* is likely due to avoidance of large changes in temperature or hydrologic cycle patterns.

[28] For most of the results presented in this study, changes in *G1* relative to *piControl* are substantially smaller than changes in *abrupt4xCO2* relative to *piControl*. However, this does not preclude the possibility that for some fields, local changes in *G1* may be larger than the projected changes for *abrupt4xCO2*. (For example, increases in terrestrial net primary productivity are larger in some regions in *G1* than in *abrupt4xCO2*.)

[29] No model shows the ability of uniform solar geoengineering to offset all climate changes from increased carbon dioxide concentration. In particular, there is a trade-off between reducing residuals (*G1–piControl*) in temperature and hydrology; this finding of *Ricke et al.* [2010] and *Moreno-Cruz et al.* [2012] is a robust feature of all models participating in GeoMIP. *MacMartin et al.* [2013] proposed other potential trade-offs, for example, between returning the hydrologic cycle to preindustrial levels and returning Arctic sea ice to preindustrial levels.

[30] Although Experiment *G1* provides important clues about fundamental climate system effects of solar geoengineering, the idealized nature of Experiment *G1* suggests the need for complementary studies that are currently underway. Other GeoMIP simulations use transient greenhouse gas profiles and stratospheric sulfate aerosols instead of solar constant reductions. Ongoing studies involving these simulations will analyze the climate responses to transient greenhouse gasses, stratospheric heating from aerosols, and the resulting dynamical circulation and chemistry changes. We also plan investigations under the GeoMIP framework of the effects of solar geoengineering on sea ice, circulation patterns, and extreme events. We also note that our results are specific to imposition of a globally uniform solar reduction. Tailoring the method of solar geoengineering, potentially including variations in latitude and season of forcing, has the potential to alter the climate effects [*MacMartin et al.*, 2013]. In this study, we have not addressed the problem of ocean acidification [e.g., *Raven et al.*, 2005], which could be exacerbated by solar geoengineering because the resulting cooler ocean would absorb more $CO_2$.

[31] The results we present are specific to the highly idealized Experiment *G1* and should neither be mistaken as an evaluation of geoengineering proposals or issues surrounding their implementation, nor as representative of how geoengineering might be implemented in practice. The potential goals of geoengineering will likely include factors other

than radiative balance or temperature reductions. In particular, the trade-off between temperature and hydrology shown above, as well as other potential trade-offs [*MacMartin et al.*, 2013], suggest that careful planning of optimal geoengineering strategies might be required to produce desired climate changes while avoiding side effects. Moreover, our analysis did not include effects on social or political structures, ecosystem dynamics, and many other potentially important issues. Such an evaluation would consider a wider range of concerns and possible deployment modalities than have been included in the scope of the GeoMIP efforts. We make efforts to present and analyze climate model simulation results without injection of moral values, but a more complete evaluation of geoengineering proposals will depend critically on societal norms and would address ethical concerns. Sound scientific and technical results such as we have presented here are thus necessary, but not sufficient, inputs for evaluating solar geoengineering proposals.

[32] **Acknowledgments.** We thank all participants of the Geoengineering Model Intercomparison Project and their model development teams, the CLIVAR/WCRP Working Group on Coupled Modeling for endorsing GeoMIP, the scientists managing the Earth System Grid data nodes who have assisted with making GeoMIP output available, and Vivek Arora, Andy Ridgwell, Georgiy L. Stenchikov, and three anonymous reviewers for helpful comments. We acknowledge the World Climate Research Programme's Working Group on Coupled Modelling, which is responsible for CMIP, and we thank the climate modeling groups (listed in Table 1) for producing and making available their model output. For CMIP, the U.S. Department of Energy's Program for Climate Model Diagnosis and Intercomparison provides coordinating support and led development of software infrastructure in partnership with the Global Organization for Earth System Science Portals. BK is supported by the Fund for Innovative Climate and Energy Research. Simulations performed by BK were supported by the NASA High-End Computing (HEC) Program through the NASA Center for Climate Simulation (NCCS) at Goddard Space Flight Center. The Pacific Northwest National Laboratory is operated for the U.S. Department of Energy by Battelle Memorial Institute under contract DE-AC05-76RL01830. AR is supported by US National Science Foundation grant AGS-1157525. JMH and AJ were supported by the joint DECC/Defra Met Office Hadley Centre Climate Programme (GA01101). KA, DBK, JEK, UN, HS, and MS received funding from the European Union's Seventh Framework Programme (FP7/2007–2013) under grant agreement 226567-IMPLICC. KA and JEK received support from the Norwegian Research Council's Programme for Supercomputing (NOTUR) through a grant of computing time. Simulations with the IPSL-CM5 model were supported through HPC resources of [CCT/TGCC/CINES/IDRIS] under the allocation 2012-t2012012201 made by GENCI (Grand Equipement National de Calcul Intensif). DJ and JCM thank all members of the BNU-ESM model group, as well as the Center of Information and Network Technology at Beijing Normal University for assistance in publishing the GeoMIP data set. The National Center for Atmospheric Research is funded by the National Science Foundation. SW was supported by the Innovative Program of Climate Change Projection for the 21st century, MEXT, Japan. Computer resources for PJR, BS, and JHY were provided by the National Energy Research Scientific Computing Center, which is supported by the Office of Science of the U.S. Department of Energy under contract DE-AC02-05CH11231.

## References

Aleinov, I., and G. Schmidt (2006), Water isotopes in the GISS ModelE land surface scheme, *Global Planet. Change*, *51*(1-2), 108–120, doi:10.1016/j.gloplacha.2005.12.010.

Alterskjær, K., J. E. Kristjansson, and Ø. Seland (2012), Sensitivity to deliberate sea salt seeding of marine clouds – Observations and model simulations, *Atmos. Chem. Phys.*, *12*, 2,795–2,807, doi:10.5194/acp-12-2795-2012.

Ammann, C. M., W. M. Washington, G. A. Meehl, L. Buja, and H. Teng (2010), Climate engineering through artificial enhancement of natural forcings: Magnitudes and implied consequences, *J. Geophys. Res.*, *115*, D22109, doi:10.1029/2009JD012878.

Arora, V. K., and G. J. Boer (2010), Uncertainties in the 20th century carbon budget associated with land use change, *Global Change Biol.*, *16*(12), 3,327–3,348, doi:10.1111/j.1365-2486.2010.02202.x.

Arora, V. K., J. F. Scinocca, G. J. Boer, J. R. Christian, K. L. Denman, G. M. Flato, V. V. Kharin, W. G. Lee, and W. J. Merryfield (2011), Carbon emission limits required to satisfy future representative concentration pathways of greenhouse gases, *Geophys. Res. Lett.*, *38*, L05805, doi:10.1029/2010GL046270.

Assmann, K. M., M. Bentsen, J. Segschneider, and C. Heinze (2010), An isopycnic ocean carbon cycle model, *Geosci. Model. Dev.*, *3*, 143–167, doi:10.5194/gmd-3-143-2010.

Bala, G., P. B. Duffy, and K. E. Taylor (2008), Impact of geoengineering schemes on the global hydrological cycle, *Proc. Natl. Acad. Sci. U. S. A.*, *105*, 7,664–7,669, doi:10.1073/pnas.0711648105.

Ban-Weiss, G. A., and K. Caldeira (2010), Geoengineering as an optimization problem, *Environ. Res. Lett.*, *5*, 034009, doi:10.1088/1748-9326/5/3/034009.

Bony, S., G. Bellon, D. Klocke, S. Sherwood, S. Fermepin, and S. Denvil (2013), Robust direct effect of carbon dioxide on tropical circulation and regional precipitation, *Nat. Geosci.*, *6*, 447–451, doi:10.1038/ngeo1799.

Budyko, M. I. (1974), *Climate and Life*, 508 pp., Academic Press, New York.

Cao, L., G. Bala, K. Caldeira, R. Nemani, and G. Ban-Weiss (2010), Importance of carbon dioxide physiological forcing to future climate change, *Proc. Natl. Acad. Sci. U. S. A.*, *107*, 9,513–9,518, doi:10.1073/pnas.0913000107.

Collins, W. J., et al. (2011), Development and evaluation of an Earth-system model—HadGEM2, *Geosci. Model. Dev.*, *4*, 1,051–1,075, doi:10.5194/gmd-4-1051-2011.

Cramer, W., et al. (1999), Comparing global models of terrestrial net primary productivity (NPP): Overview and key results, *Global Change Biol.*, *5*, 1–15, doi:10.1046/j.1365-2486.1999.00009.x.

Crutzen, P. J. (2006), Albedo enhancement by stratospheric sulfur injections: A contribution to resolve a policy dilemma?, *Clim. Change*, *77*(3–4), 211–220, doi:10.1007/s10584-006-9101-y.

Dai, Y., et al. (2003), The Common Land Model (CLM), *Bull. Am. Meteorol. Soc.*, *84*, 1,013–1,023, doi:10.1175/BAMS-84-8-1013.

Dai, Y., R. E. Dickinson, and Y.-P. Wang (2004), A two-big-leaf model for canopy temperature, photosynthesis, and stomatal conductance, *J. Clim.*, *17*, 2,281–2,299, doi:10.1175/1520-0442(2004)017<2281:ATMFCT>2.0.CO;2.

Dufresne, J.-L., et al. (2013), Climate change projections using the IPSL-CM5 Earth System Model: From CMIP3 to CMIP5, *Clim. Dyn.*, *40*, 2,123–2,165, doi:10.1007/s00382-012-1636-1.

Essery, R. L. H., M. J. Best, R. A. Betts, P. M. Cox, and C. M. Taylor (2003), Explicit representation of subgrid heterogeneity in a GCM land surface scheme, *J. Hydrometeorol.*, *4*, 530–543, doi:10.1175/1525-7541(2003)004<0530:EROSHI>2.0.CO;2.

Field, C., R. Jackson, and H. Mooney (1995), Stomatal responses to increased $CO_2$: Implications from the plant to the global scale, *Plant, Cell Environ.*, *18*, 1,214–1,255, doi:10.1111/j.1365-3040.1995.tb00630.x.

Fyfe, J. C., J. N. S. Cole, V. K. Arora, and J. F. Scinocca (2013), Biogeochemical carbon coupling influences global precipitation in geoengineering experiments, *Geophys. Res. Lett.*, *40*, 651–655, doi:10.1002/grl.50166.

Gent, P. R., et al. (2011), The Community Climate System Model 4, *J. Clim.*, *24*, 4,973–4,991, doi:10.1175/2011JCLI4083.1.

Giorgetta, M. A., et al. (2013), Climate and carbon cycle changes from 1850 to 2100 in MPI-ESM simulations for the coupled model intercomparison project phase 5, *J. Adv. Model. Earth Syst.*, doi:10.1002/jame.20038, in press.

Gordon, C., et al. (2000), The simulation of SST, sea ice extents and ocean heat transports in a version of the Hadley Centre coupled model without flux adjustments, *Clim. Dyn.*, *16*(2-3), 147–168, doi:10.1007/s003820050010.

Govindasamy, B., and K. Caldeira (2000), Geoengineering Earth's radiation balance to mitigate $CO_2$-induced climate change, *Geophys. Res. Lett.*, *27*, 2,141–2,144, doi:10.1029/1999GL006086.

Govindasamy, B., S. Thompson, P. B. Duffy, K. Caldeira, and C. Delire (2002), Impact of geoengineering schemes on the terrestrial biosphere, *Geophys. Res. Lett.*, *29*, 2061, doi:10.1029/2002GL015911.

Hazeleger, W., et al. (2011), EC-Earth V2.2: Description and validation of a new seamless Earth system prediction model, *Clim. Dyn.*, *39*(11), 2,611–2,629, doi:10.1007/s00382-011-1228-5.

Held, I. M., and B. J. Soden (2006), Robust responses of the hydrological cycle to global warming, *J. Clim.*, *19*, 5,686–5,699, doi:10.1175/JCLI3990.1.

Hourdin, F., et al. (2012), Impact of the LMDZ atmospheric grid configuration on the climate and sensitivity of the IPSL-CM5A coupled model, *Clim. Dyn.*, *40*, 2167–2192, doi:10.1007/s00382-012-1411-3.

Huntington, T. G. (2006), Evidence for intensification of the global water cycle: Review and synthesis, *J. Hydrol.*, *319*(1–4), 83–95, doi:10.1016/j.hydrol.2005.07.003.

IPCC (2007), *Climate Change 2007: Synthesis Report. Contribution of Working Groups I, II and III to the Fourth Assessment Report of the Intergovernmental Panel on Climate Change*, edited by Core Writing

Team, R. K. Pachauri, and A. Reisinger, 104 pp., IPCC, Geneva, Switzerland.
Jones, A., J. Haywood, O. Boucher, B. Kravitz, and A. Robock (2010), Geoengineering by stratospheric $SO_2$ injection: Results from the Met Office HadGEM2 climate model and comparison with the Goddard Institute for Space Studies ModelE, *Atmos. Chem. Phys.*, *10*, 5,999–6,006, doi:10.5194/acp-10-5999-2010.
K-1 model developers (2004), K-1 Coupled GCM (MIROC) Description, *K-1 Technical Report No. 1* (Center for Climate System Research, National Institute for Environmental Studies, and Frontier Research Center for Global Change), available online at http://www.ccsr.u-tokyo.ac.jp/kyosei/hasumi/MIROC/tech-repo.pdf.
Kirkevåg, A., et al. (2013), Aerosol-climate interactions in the Norwegian Earth System Model—NorESM1-M, *Geosci. Model. Dev.*, *6*, 207–244, doi:10.5194/gmd-6-207-2013.
Kravitz, B., A. Robock, O. Boucher, H. Schmidt, K. E. Taylor, G. Stenchikov, and M. Schulz (2011a), The Geoengineering Model Intercomparison Project (GeoMIP), *Atmos. Sci. Lett.*, *12*, 162–167, doi:10.1002/asl.316.
Kravitz, B., A. Robock, O. Boucher, H. Schmidt, and K. E. Taylor (2011b), Specifications for GeoMIP experiments *G1* through *G4* (Version 1.0), available online at http://climate.envsci.rutgers.edu/GeoMIP/docs/specificationsG1_G4_v1.0.pdf.
Krinner, G., N. Viovy, N. de Noblet-Ducoudré, J. Ogée, J. Polcher, P. Friedlingstein, P. Ciais, S. Sitch, and I. C. Prentice (2005), A dynamic global vegetation model for studies of the coupled atmosphere-biosphere system, *Global Biogeochem. Cycles*, *19*, GB1015, doi:10.1029/2003GB002199.
Lunt, D. J., A. Ridgwell, P. J. Valdes, and A. Seale (2008), "Sunshade World": A fully coupled GCM evaluation of the climatic impacts of geoengineering, *Geophys. Res. Lett.*, *35*, L12710, doi:10.1029/2008GL033674.
MacMartin, D. G., D. W. Keith, B. Kravitz, and K. Caldeira (2013), Management of trade-offs in geoengineering through optimal choice of non-uniform radiative forcing, *Nat. Clim. Change*, *3*, 365–368, doi:10.1038/nclimate1722.
Madec, G. (2008), NEMO ocean engine. Tech. Rep. 27, Institut Pierre Simon Laplace des Sciences d l'Environement Global (Paris).
Marsland, S. J., H. Haak, J. H. Jungclaus, M. Latif, and F. Röske (2003), The Max-Planck-Institute global ocean/sea ice model with orthogonal curvilinear coordinates, *Ocean Model.*, *5*, 91–127.
Mercado, L. M., et al. (2009), Impact of changes in diffuse radiation on the global land carbon sink, *Nature*, *458*, 1,014–1,018, doi:10.1038/nature07949.
Moreno-Cruz, J. B., K. L. Ricke, and D. W. Keith (2012), A simple model to account for regional inequalities in the effectiveness of solar radiation management, *Clim. Change*, *110*, 649–668, doi:10.1007/s10584-011-0103-z.
Naik, V., D. J. Wuebbles, E. H. DeLucia, and J. A. Foley (2003), Influence of geoengineered climate on the terrestrial biosphere, *Environ. Manage.*, *32*(3), 373–381, doi:10.1007/s00267-003-2993-7.
Oleson, K. W., et al. (2010), Technical description of version 4.0 of the Community Land Model (CLM), NCAR Technical Note NCAR/TN-478+STR, National Center for Atmospheric Research.
Pongratz, J., D. B. Lobell, L. Cao, and K. Caldeira (2012), Crop yields in a geoengineered climate, *Nat. Clim. Change*, *2*, 101–105, doi:10.1038/nclimate1373.
Potter, C., S. Klooster, and V. Genovese (2012), Net primary production of terrestrial ecosystems from 2000 to 2009, *Clim. Change*, *115*, 365–378, doi:10.1007/s10584-012-0460-2.
Raddatz, T. J., C. H. Reick, W. Knorr, J. Kattge, E. Roeckner, R. Schnur, K.-G. Schnitzler, P. Wetzel, and J. Jungclaus (2007), Will the tropical land biosphere dominate the climate–carbon cycle feedback during the twenty-first century?, *Clim. Dyn.*, *29*(6), 565–574, doi:10.1007/s00382-007-0247-8.
Ramanathan, V., R. D. Cess, E. F. Harrison, P. Minnis, B. R. Barkstrom, E. Ahmad, and D. Hartmann (1989), Cloud-radiative forcing and climate: Results from the Earth radiation budget experiment, *Science*, *243*, 57–63.
Rasch, P. J., et al. (2008), An overview of geoengineering the climate using stratospheric sulfate aerosols, *Phil. Trans. Roy. Soc. A*, *366*, 4,007–4,037, doi:10.1098/rsta.2008.0131.
Rasch, P. J., J. Latham, and C.-C. Chen (2009), Geoengineering by cloud seeding: Influence on sea ice and climate system, *Environ. Res. Lett.*, *4*(4), 045112, doi:10.1088/1748-9326/4/4/045112.
Raven, J., et al. (2005), *Ocean Acidification Due to Increasing Atmospheric Carbon Dioxide*. Policy Document 12/05, 68 pp., The Royal Society, London, UK.
Ricke, K. L., M. G. Morgan, and M. R. Allen (2010), Regional climate response to solar-radiation management, *Nat. Geosci.*, *3*, 537–541, doi:10.1038/ngeo915.
Robock, A. (2000), Volcanic eruptions and climate, *Rev. Geophys.*, *38*, 191–219, doi:10.1029/1998RG000054.
Russell, G. L., J. R. Miller, and D. Rind (1995), A coupled atmosphere-ocean model for transient climate change, *Atmos.-Ocean*, *33*, 683–730.
Schimel, D. S. (1995), Terrestrial ecosystems and the carbon cycle, *Global Change Biol.*, *1*(1), 77–91, doi:10.1111/j.1365-2486.1995.tb00008.x.
Schmidt, G. A., et al. (2006), Present-day atmospheric simulations using GISS ModelE: Comparison to in situ, satellite and reanalysis data, *J. Clim.*, *19*, 153–192, doi:10.1175/JCLI3612.1.
Schmidt, H., et al. (2012a), IMPLICC: Implications and risks of engineering solar radiation to limit climate change: Synthesis report for policy makers and the interested public, available online at http://implicc.zmaw.de/fileadmin/user_upload/implicc/deliverables/D6_3_synthesis_report_nohead.pdf.
Schmidt, H., et al. (2012b), Solar irradiance reduction to counteract radiative forcing from a quadrupling of $CO_2$: Climate responses simulated by four earth system models, *Earth Syst. Dyn.*, *3*, 63–78, doi:10.5194/esd-3-63-2012.
Sellers, P. J., et al. (1996), Comparison of radiative and physiological effects of doubled atmospheric $CO_2$ on climate, *Science*, *271*, 1,402–1,406.
Shepherd, J., et al. (2009), Geoengineering the climate: Science, governance, and uncertainty. Royal Society Policy document 10/09, 82 pp.
Smith, R. D., et al. (2010), The Parallel Ocean Program (POP) reference manual, Los Alamos National Laboratory Tech. Rep. LAUR-10-01853.
Stevens, B., et al. (2013), The atmospheric component of the MPI-M Earth System Model: ECHAM6, *J. Adv. Model. Earth Syst.*, *5*, doi:10.1002/jame.20015.
Stroeve, J. C., M. C. Serreze, M. M. Holland, J. E. Kay, J. Malanik, and A. P. Barrett (2012), The Arctic's rapidly shrinking sea ice cover: A research synthesis, *Clim. Change*, *110*(3-4), 1,005–1,027, doi:10.1007/s10584-011-0101-1.
Takata, K., S. Emori, and T. Watanabe (2003), Development of the minimal advanced treatments of surface interaction and runoff, *Global Planet. Change*, *38*(1-2), 209–222, doi:10.1016/S0921-8181(03)00030-4.
Taylor, K. E., R. J. Stouffer, and G. A. Meehl (2012), An overview of CMIP5 and the experiment design, *Bull. Am. Meteorol. Soc.*, *93*, 485–498, doi:10.1175/BAMS-D-11-00094.1.
The HadGEM2 Development Team (2011), The HadGEM2 family of Met Office Unified Model climate configurations, *Geosci. Model. Dev.*, *4*, 723–757, doi:10.5194/gmd-4-723-2011.
Verseghy, D., N. A. McFarlane, and M. Lazare (1993), CLASS – A Canadian land surface scheme for GCMs, II: Vegetation model and coupled runs, *Int. J. Climatol.*, *13*, 347–370.
Watanabe, S., et al. (2008), Development of an atmospheric general circulation model for integrated Earth system modeling on the Earth Simulator, *J. Earth Simulator*, *9*, 27–35.
Watanabe, S., et al. (2011), MIROC-ESM 2010: Model description and basic results of CMIP5-20c3m experiments, *Geosci. Model Dev.*, *4*, 845–872, doi:10.5194/gmd-4-845-2011.
Wigley, T. M. L. (2006), A combined mitigation/geoengineering approach to climate stabilization, *Science*, *314*(5798), 452–454, doi:10.1126/science.1131728.
Zelinka, M. D., S. A. Klein, and D. L. Hartmann (2012), Computing and partitioning cloud feedbacks using cloud property histograms. Part I: Cloud radiative kernels, *J. Clim.*, *25*, 3,715–3,735, doi:10.1175/JCLI-D-11-00248.1.